Journal of Environmental Chemical Engineering 9 (2021) 104934

Contents lists available at ScienceDirect

Journal of Environmental Chemical Engineering

journal homepage: www.elsevier.com/locate/jece

Research paper

Novel onion-like carbon structures modified with iron oxide as photocatalysts for the degradation of persistent pollutants

C.G. Renda [a], L.A. Goulart [b], C.H.M. Fernandes [c], L.H. Mascaro [c], J.M. de Aquino [c], R. Bertholdo [d,*]

[a] Federal University of São Carlos, Materials Engineering Department, Washington Luiz Highway, km 235, São Carlos, SP 13565 905, Brazil
[b] University of São Paulo, São Carlos Institute of Chemistry, Trabalhador São Carlense Avenue, 400, Parque Arnold Schimidt, São Carlos, SP 13566 590, Brazil
[c] Federal University of São Carlos, Chemistry Department, Washington Luiz Highway, km 235, São Carlos, SP 13565 905, Brazil
[d] Federal University of Alfenas, Institute of Science and Technology, José A. Vilela Highway, 11999, BR 267, Km 533, Poços de Caldas, MG 37715 400, Brazil

ARTICLE INFO

Keywords:
Phenolic resins
Onion-like carbon structures
Iron oxides
Photocatalyst
Methylene blue

ABSTRACT

A new photocatalyst based on onion-like carbon structures has been designed by heat-treating a modified phenolic resin (PR) modified with ferrocene (Fc). Its photocatalytic activity was investigated by degrading the methylene blue (MB) dye in the presence of UV–vis light. The catalyst was characterized by X-ray diffraction (XRD), Transmission Electron Microscopy (TEM) and Diffuse Reflectance Spectroscopy (DRS) moreover, the Brunauer-Emmett-Teller (BET) method was used to calculate the surface area. The carbon-iron catalyst (PR-Fc) presents high surface area and its structure is composed of amorphous carbon, graphite, γ-iron, Fe_3C (cementite), α-Fe_2O_3 (hematite), and γ-Fe_2O_3 (maghemite). The results indicate 100% of dye degradation and removal of 97% of the organic load after just 60 min of reaction. The catalytic efficiency of PR-Fc for degradation was maintained in reuse experiments, with a decrease of only 23% after the third cycle. The PR-Fc photocatalyst is reusable and quite stable, thus it has enormous potential for treating organic pollutants.

1. Introduction

In recent years, emerging contaminants such as drugs, personal care products, dyes, and pesticides have been receiving extensive attention due to their accumulation in the environment [1,2]. Dyes correspond to a large part of those substances discharged by industries in effluents that contaminate surface waters, bringing risks to the aquatic living beings in addition to possible effects on human health [3,4]. The dyes can cause dermatitis, allergies, mutagenic effects in aquatic and human organisms, and are associated with the appearance of some types of cancer [5,6]. Methylene blue (MB) is a dye widely used mainly for printing fabric, cotton, and tannins, and also as an indicator for dyeing leather [7]. The widespread use of this dye and improper discharge into the environment can lead to its bioaccumulation, causing serious damage to aquatic biomes. Thus, developing technologies for the treatment of contaminated water and wastewater containing this type of recalcitrant pollutant is necessary.

Processes for the treatment of water and effluents such as Electro-Fenton (EF) [8], Fenton, Fenton like and photo-assisted Fenton processes [9–12] are widely used. However, the EF process can be costly, while the Fenton and Fenton-like processes can generate precipitates depending on the working pH [13–15]. UV radiation can be combined with Fenton or Fenton-like processes enhancing the biodegradability of wastewater and improving the efficiencies of organic dye degradation and of the mineralization of recalcitrant contaminants [11,16,17]. Advanced Oxidation Processes exhibit good performance in removing emerging contaminants, due to the high oxidizing capacity of the hydroxyl radicals (•OH), therefore, they have been widely used to remove persistent organic compounds present in wastewater [18].

The heterogeneous photocatalysis has been shown to be part of a potential solution to convert photon energy into chemical energy, although there are challenges such as the solar energy conversion and the suppression of recombination of electron-hole pairs [19]. Moreover, many studies have been developed to identify the secondary products generated from photodegradation techniques, due to the possibility of toxic products [20].

The combination of adsorption/photodegradation promises to remove or eliminate the dye from the water [20]. The advantages of

* Corresponding author.
E-mail address: roberto.bertholdo@unifal-mg.edu.br (R. Bertholdo).

https://doi.org/10.1016/j.jece.2020.104934
Received 22 October 2020; Received in revised form 24 November 2020; Accepted 9 December 2020
Available online 13 December 2020

adsorption are high selectivity, high efficiency, facile processing, absence of harsh chemicals, high productivity, high cost-effectivity ratio, easy post-treatment, less disruptive nature, [2] and reusability without by-products. Carbon nanomaterials characteristically have unique porous structures, large surface area, hydrophobic nature, high stability [21,22], and functional groups on carbon surfaces [23]. Moreover, the introduction of other species, such as ferric chloride ($FeCl_3$), can induce the production of activated carbons with smaller pore sizes and greater surface areas upon chemical activation, which results in more efficient adsorbent catalysts [21,24,25]. It is important to mention that the use of ultra-processed and advanced materials such as the other forms of carbon (namely, carbon nanotubes, Graphene Oxide, and other graphene-based materials) can suppress the low-cost label [20] often associated with environmentally-friendly behavior expected in adsorption and photocatalytic methods.

The photodegradation-based removal of a variety of organic pollutants from wastewater has been studied. Several nanomaterials can be applied to methylene blue dye (MB) removal, such as Ag [26], Sn, metal oxides (for example, ZnO [27], iron oxides [4,7,13,28–30], SiO_2, SnO_2 [31,32], TiO_2), and others. They are activated under the irradiation of light with different wavelengths [33,34]. One explanation may be that nanoparticles such as TiO_2, SiO_2, carbon nanotubes, and others promote a reduction of interfacial tension and much higher surface activity due their atoms in the surface. In addition, nanoparticles have the amphiphilic quality, attracting hydrophilic and hydrophobic molecules, but this interaction requires time to occur and decreases with time [22,35,36].

Nanotechnology can be employed in water purification because it is efficient, cost-effective and accurate. Nanoengineered materials with hybrid compositions have been attracting attention of the researchers due the balance between applicability and control. As an example, the combination of the electronic properties of the graphene environment and the properties of transition-metal complexes can strongly influence the catalytic efficiency.

Among the photocatalysts that have been studied in recent years, materials based on carbon and iron stand out for presenting good adsorption and catalytic efficiency. In this sense, onion-like carbon structures with iron oxides between carbon lamellae and crystals in carbon matrices have been obtained from another study carried out by our group [37]. The material presented interesting conduction, magnetic and physicochemical properties for application in the removal of dyes from wastewater. The material presented cementite, γ-iron, maghemite, and hematite when treated at 1000 °C for 5 h [37]. Another key feature of material is the presence of the great number of active sites that can interact with dye molecules through adsorption [20] simultaneously to the absorption of photons, resulting in an efficient photomineralization [38].

Thus, the aim of this study was to use an organized carbon material, designed from a modified phenolic resin synthesized with ferrocene (PR-Fc), to evaluate its photocatalytic activity during the degradation of the MB dye under UV-Vis light. The influence of the catalyst mass and its reuse were investigated, and a possible MB degradation mechanism is proposed using the PR-Fc catalyst in the presence of UV-Vis light during the degradation.

2. Experimental

2.1. Materials and methods

All chemicals and reagents were of analytical grade. Methylene blue was purchased from Synth. Phenol (99% purity) and formaldehyde (37% w/w, density of 1.08 g cm^{-3}) were purchased from Proquimios (Brazil). Hydrochloric acid (37% w/w) was supplied by Vetec (Brazil). Ferrocene (98% purity and 150<d<70 μm) was acquired from Aldrich (USA). Deionized water (Millipore Milli-Q system, resistivity ≤18.2 MΩ cm) was used for the preparation of all solutions.

2.2. Synthesis of PR-Fc materials

A phenolic resin (PR) called "modified novolak" synthesized in the laboratory, was obtained by the following procedure: first, phenol and formaldehyde (in 0.33 molar ratio) were magnetically stirred for 30 min; then, a catalytic acid was added (ratio of 0.67 vol hydrochloric acid: formaldehyde) and the material remained under stirring for additional 90 min until two phases were obtained according to previous researches [39–41]. A separating funnel was used to remove the bottom phase containing the pre-polymer, which was weighed. Then, ferrocene (Fc) was added (3 wt%) using a vertical lab mixer (for 20 min) and an ultrasonic probe (for 10 min). The material underwent heat treatment at the temperatures of 80 °C for 120 min, 100 °C for 30 min, 150 °C for 30 min, 200 °C for 60 min, 500 °C for 60 min, and 1000 °C for 300 min; then, it was cooled to room temperature in a tubular furnace under reducing atmosphere (simulated by a refractory box containing coke) at a heating rate of 3 °C per minute. The heat treatment and the additive to control the catalytic graphitization process were defined in previous studies [37,40].

2.3. Characterization of the PR-Fc photocatalyst

The PR-Fc samples were ground and the resulting powders were evaluated by powder X-Ray Diffraction (XRD) measurements employing a Bruker XRD 8 Advance equipment using CuKα radiation [1.5406 Å] and a 2θ range from 10 to 80 degrees with step size = $0.02^{\circ} \times sec^{-1}$.

Transmission electron microscopy (TEM) analyses were performed on a Tecnai G2F20-with Energy Dispersive X-Ray Spectrometer (EDS) and Mapping. Powders of the samples were solubilized in isopropyl alcohol and dispersed using an ultrasonic mixer for 30 min. Afterwards, the materials were deposited on copper and carbon grids and dried for 24 h in a desiccator.

The Diffuse Reflectance ultraviolet-visible Spectroscopy (DRS) technique was used to obtain optical information about the materials. It was opted for diffuse reflectance, since it allows determination of the band gap by the Tauc plot method [42]. Measurements were performed at room temperature and the wavelength ranged from 250 to 1000 nm in a *Shimadzu* UV-Vis spectrophotometer model UV-2600 in diffuse reflectance mode, moreover, the Kubelka-Munk equation was employed, where hυ = photon energy, namely 1239.7 nm for lambda (λ), which is the wavelength of the incident light.

The porosity of the samples was assessed by Nitrogen physisorption using a Micromeritics Gemini VII equipment. About 500 mg of powder was previously treated at 350 °C under a vacuum atmosphere in a Micromeritics Vap Prep 061 Sample Degas System. Measurements were performed and the gas-phase isotherm physisorption curves were obtained for the PR-Fc samples. The specific surface area was obtained using the Brunauer-Emmett-Teller (BET) method for a region of $P/P_0 \leq 0.3$.

2.4. Photocatalytic activity test

A photocatalytic activity test was performed during the degradation of the methylene blue (MB) dye in an aqueous solution under UV-Vis light irradiation (125 W, Philips). All experiments lasted 60 min using 200 mL of MB solution at the concentration of 25 mg L^{-1}. Afterwards, the solution was left in equilibrium in the dark and the catalyst remained under magnetic stirring for 5 min. Experiments were carried out in a termostatized glass cell with central illumination. The cell was covered with a black box to avoid external light incidence and all experiments were performed at 25 °C using a thermostatic bath.

The influence of catalyst mass (10, 20 and 40 mg) and type (PR and PR-Fc) on the photocatalytic degradations were studied. Adsorption and desorption studies were carried out, thus, after the photocatalysis, the catalysts remained under magnetic stirring for 1 h in the same solution used during the photocatalysis process, afterwards, desorption tests

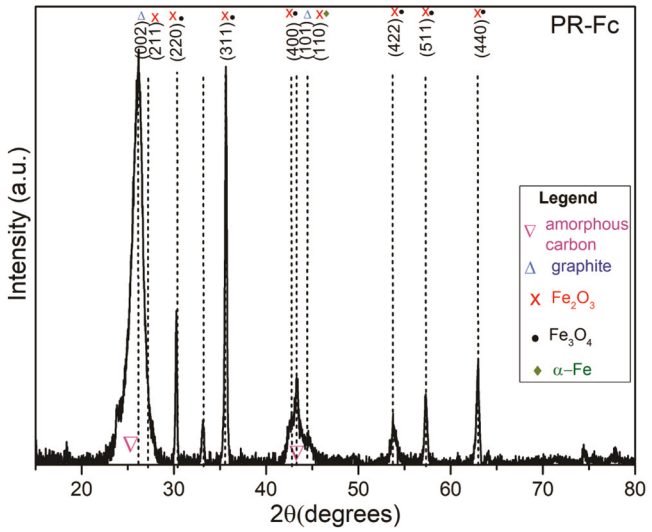

Fig. 1. XRD results of PR-Fc powder after heat treatment up to 1000 °C.

were performed with addition of 25 mL of acetonitrile 99.9% and 25 mL of ethanol 99.8%. Eqs. (1) and (2) were used to evaluate the percentage of adsorption and desorption of PR-Fc, respectively:

$$\%\text{Adsorption} = \left(\text{Ab}_0 - \text{Ab}_f\right) \times 100/\text{Ab}_0 \quad (1)$$

$$\%\text{Desorption} : \left(\text{Ab}_{f(des)} - \text{Ab}_f\right) \times 100/\left(\text{Ab}_0 - \text{Ab}_f\right) \quad (2)$$

where Ab_0 is the initial absorbance and Ab_f the final absorbance from the adsorption experiments, and $\text{Ab}_{f(des)}$ is the final absorbance from the desorption experiment. The catalyst reuse was also evaluated.

MB degradation was monitored by absorbance measurements using a Varian spectrophotometer model Cary 5 G/UV-Vis-NTR operating from 200 to 800 nm. The characteristic absorption band of MB at 664 nm was used to monitor the MB degradation and the results were used in the kinetic studies. The concentration of total organic carbon (TOC) was obtained using a Sievers InnovOx Laboratory TOC analyzer from GE Analytical Instruments with a GE Autosampler. The aliquots used for the UV-Vis and TOC analyses were centrifuged and filtered using a 0.22 μm filter before each measurement.

3. Results and discussion

3.1. Characterization of the PR-Fc photocatalyst

Carbonaceous materials with properties close to those of graphitic lamellae (or graphene sheets) normally are obtained in temperatures above 2000 °C [43]. Our group synthesized the turbostratic material via catalytic graphitization [37], where a mixture of a thermosetting resin (in our case phenolic chemically modified) and additives (as ferrocene) received a controlled heat treatment to improve properties such as thermal resistance and microstructure. Ferrocene improved the graphitization of the phenolic resin; furthermore, during the decomposition of PR-Fc, iron was released from the sandwich structure of ferrocene [37].

The steps of the isotherms are as important as the final temperature, since the rearrangements of the chemical structure occur at predetermined intervals, which must have sufficient time and temperature to form the ideal number of crosslinks and adjust the mobility of the carbon structure to reorganize the graphitic lamellae. Characterizations of the PR, heat treatment effects during the graphitization process, and the best additive to induce the graphitization were presented in previous studies [37,40].

From to the XRD profiles of the samples, the phases were identified using the Inorganic Crystal Structure Database (ICSD). The phases (α-iron, Fe_3O_4, Fe_2O_3, and graphite) and their corresponding planes are presented in Fig. 1.

The procedure described in [40] was used to calculate the graphitization level (GL) through Eq. (3) by considering non-graphitic peaks, $2\theta = 24°$ and 42°, as well as graphitic peaks, $2\theta = 26°$ and 44.2° corresponding to (002) and (101) planes, respectively.

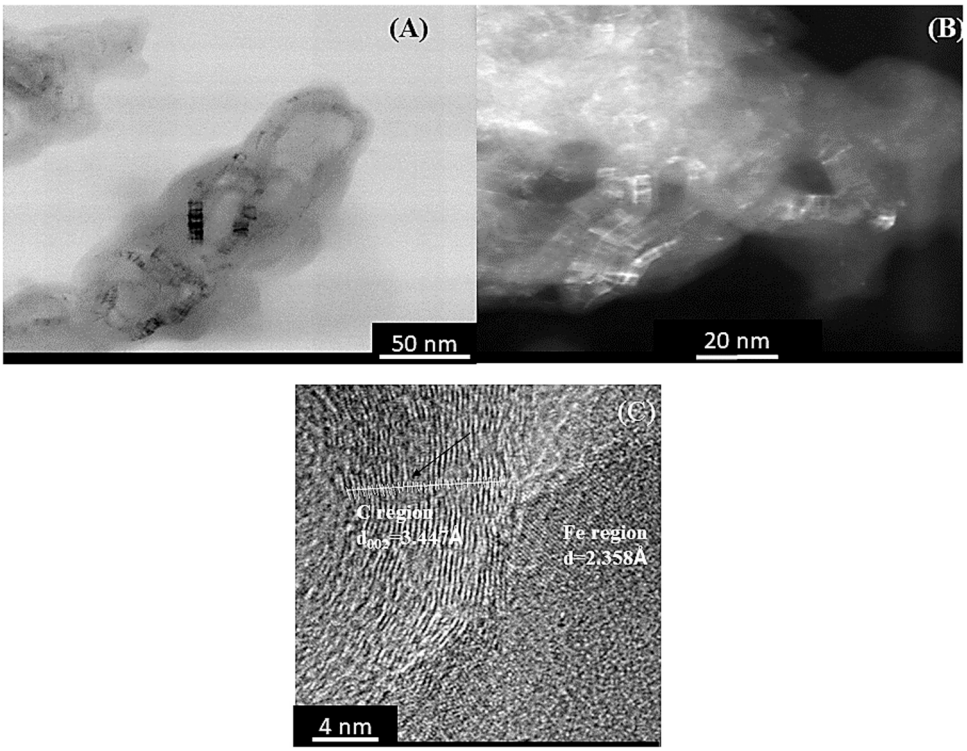

Fig. 2. PR-Fc sample Micrographs: (A) TEM Bright Field mode (BF); (B) TEM DarkField (DF); (C) HRTEM.

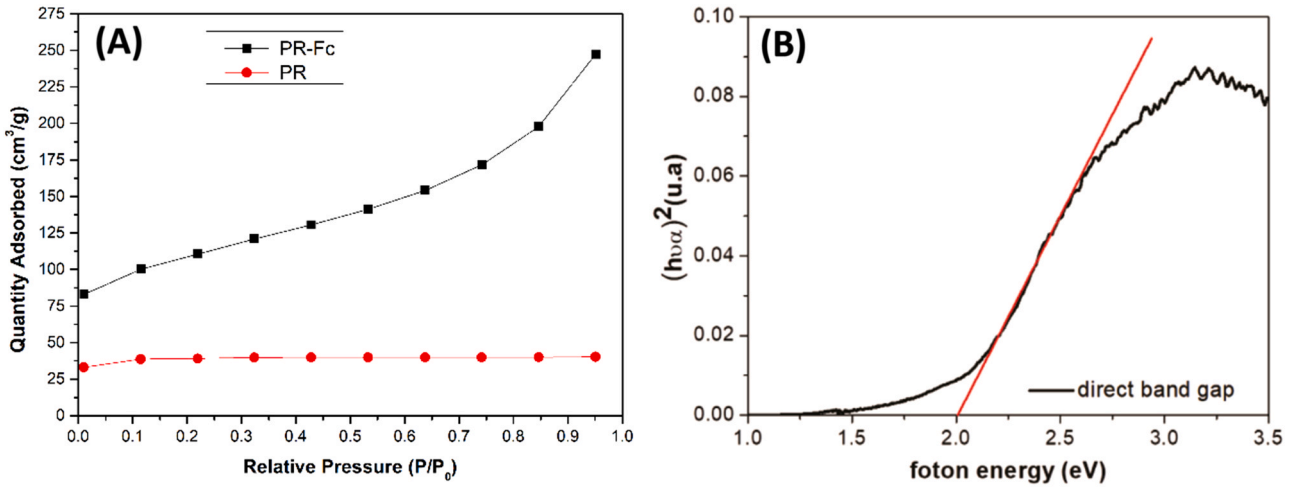

Fig. 3. (A) Nitrogen physisorption isotherm for PR-Fc and PR; (B) Tauc plot method used to determine the direct band gap of the PR-Fc sample treated up to 1000 °C.

$$GL(\%) = 100x\frac{Graphiticcarbonareas}{Totalarea \quad (graphitic + non - graphiticcarbon)} \tag{3}$$

Bragg's Law was used to calculate the interplanar distance between the iron oxide and graphitic phases and Scherrer equation was used to calculate the crystallite size of iron oxide phases and graphitic phases.

For graphitic carbon, which corresponds to the peak at $2\theta \cong 26.11^0$, the graphitization level was 70% and the interplanar distance (d_{hkl}) and crystallite size values (L_c) were of $d_{002} = 3.410$ Å and $L_c = 0.949$ Å. According to Oya and Marsh [44], those characteristics correspond to a turbostratic material, not to a three-dimensionally ordered graphitic structure. The presence of iron [37], oxide and iron phases, (400) and (110), and amorphous carbon ($2\theta \cong 24°$ and 42°) might have affected the GL calculation.

Although the XRD results showed planes coincident with hematite (α-Fe_2O_3) and magnetite (Fe_3O_4), Fe-Mossbauer measurements presented in a previously study only revealed the presence of maghemite (γ-Fe_2O_3) and hematite (α-Fe_2O_3), in addition to cementite and γ-iron [45]. For γ-Fe_2O_3 at $2\theta \cong 35.64°$, the interplanar distance and the crystallite size were of $d_{311} = 2.517$ Å and $L_c = 4.179$ Å, while edge parameter was of 8.348 Å.

Fig. 2(A) shows TEM images of the PR-Fc samples treated up to 1000 °C in Bright Field mode, in which the onion-like carbon structures are presented in gray and iron oxides organized within the carbon lamellae are presented in black. Fig. 2(B) shows the magnification of another area of the same sample in Dark Field microscopy. It is worth mentioning the organization of iron oxides in carbon ribbons. As cited before [37], these iron oxides were cementite, gamma-iron, maghemite and hematite when treated at 1000 °C/5 h. In the previous study [37], TEM images showed the interlamellar distance and electron diffraction images that confirmed the onion-like carbon structures.

Fig. 2(C) presents a TEM image in which the interlamellar distance of the carbon region was of 0.3447 nm (shown by a black arrow) and the interlamellar distance of the iron region was of 0.2358 nm, thus, corroborating the results found by Dar et al. [45] regarding Fe_2O_3 (hematite). Fe and Fe_2O_3 regions were in direct contact with a carbon region.

TEM images of the turbostratic samples are not clear enough because the onion-like carbon material has curved, semi-circular, and circular regions with carbon organized in planes similar to the graphite structure in order to minimize their surface energy, corroborating the images of references [44,46–48].

Fig. 3(A) presents results from the Brunauer-Emmett-Teller (BET) method and Fig. 3(B) shows the band gap values obtained using the Kubelka-Munk equation.

Fig. 3(A) shows the gas-phase physisorption isotherms obtained for the PR and PR-Fc samples. According to the IUPAC classification [49], the PR sample presents type I features, which show isotherms that resemble the physisorption of gases on materials having mainly narrow micropores. Differently, the PR-Fc sample shows type II features, presenting isotherms that resemble the physisorption of gases on nonporous or macroporous adsorbent materials. The BET surface area (BET_{SA}) of the PR sample without iron modification was of 118 $m^2\ g^{-1}$ and its pore size was of 24.3 Å. For the PR-Fc sample, the BET_{SA} was of 358 $m^2\ g^{-1}$ and the pore size was of 40,6 Å. Therefore, the values are increased for iron-activated species.

The increase in the BET_{SA} may be related to the formation of defects in the lattice of carbonaceous materials from non-covalent interactions with Fe or Fe complex during the decomposition of ferrocene in the lattice [41]. The catalyst synthesis method and the acidic or basic nature of the material can also influence the production of active sites and a larger surface area [42]. Thus, the increase in the surface area of the PR-Fc compared to the PR can be associated with the structural and morphological changes caused by the graphitization induced by ferrocene.

The opposite occurred in a study carried out by Chen et al. [50]. For raw activated carbon-based catalysts, the BET_{SA} and average pore diameter values were of 912 $m^2\ g^{-1}$ and 55 Å, respectively, moreover, those values decreased to 776 $m^2\ g^{-1}$ and 33.9 Å for activated carbon containing iron and cerium. The BET_{SA} values of Fe_2O_3-supported activated carbon decreased as the microporosity ranged from 750 to 150 $m^2\ g^{-1}$ and the mesoporosity ranged from 830 to 360 $m^2\ g^{-1}$ [30].

As observed in this work, Fig. 3(B) shows the direct band gap obtained from the DRS using the Tauc plot method [42] for PR-Fc materials with a photon energy of 2.0 eV, which is probably due to hematite or maghemite. Other results found in literature were 4.2 eV for γ-Fe_2O_3 [51] and around 2.1 eV for iron oxides [52]. Moreover, for the controlled synthesis of α-Fe_2O_3 and γ-Fe_2O_3 the photon energy ranged from 2.2 eV to 2.3 eV [53]. Other studies [54–56] affirmed the effectiveness of iron species (Fe_2O_3, Fe_3C, Fe_3O_4) in photocatalytic processes under UV and visible-light incidence, according to the band gap obtained for each iron species.

3.2. Photoactivity of the catalysts

The photocatalytic activity of the PR-Fc catalyst was evaluated by degrading 200 mL of MB, 25 mg L^{-1}, under light irradiation monitoring the system by UV–vis spectroscopy. This MB concentration was chosen based on the average dye concentration generally reported in the literature with other catalysts (5–100 mg L^{-1}) [7,13,57]. Dariani et al. showed that the efficiency of decomposition of MB is directly related to

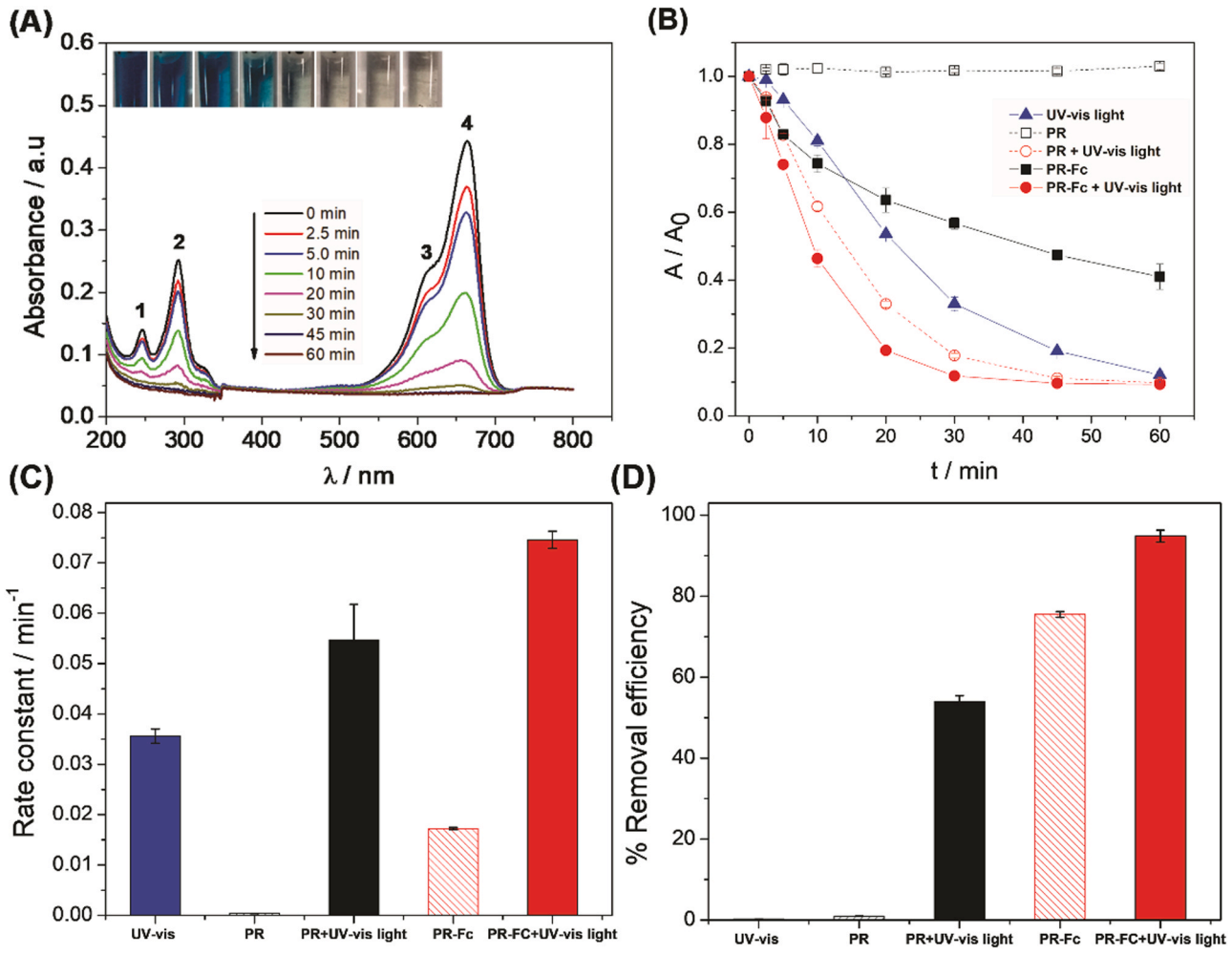

Fig. 4. (A) MB UV-Vis absorption spectra at different photocatalysis times. (B) MB degradation in the presence of combinations of PR, PR-Fc and UV-Vis light. (C) Graph showing the rate constant for each studied system. (D) MB percent removal efficiency in the presence of combinations of PR, PR-Fc and UV-Vis light. The error bars correspond to two repetitions.

the initial concentration of the dye, where the degradation of MB decreased with increasing concentration. Besides, UV light can pass through diluted solutions more easily, facilitating the photo-activation of the photocatalyst [58].

The MB absorption spectra in the presence of PR-Fc and light are shown in Fig. 4(A) for different degradation times. The top of Fig. 4(A) corresponds to the discoloration of the solution as degradation occurs. Four MB absorption bands were observed in a 200–800 nm range. The characteristic bands of MB at 664 nm (4) and 612 nm (3), in the visible region, are related to the sulfur-nitrogen conjugate system acting as a chromophore [3]. As the degradation reaction progresses, the intensities of those bands decrease, which indicates that the sulfur and nitrogen conjugate system was destroyed. Thus, a gradual decrease in the coloration of the MB solution is observed over time. The discoloration of the MB solution can also be related to the demethylation of MB molecules that convert into other intermediates. The bands in the UV region at 292 nm (2) and 246 nm (1) correspond to the phenothiazine group present in the MB molecules [59]. A gradual decrease of these bands was also observed throughout the degradation, which is possibly related to the oxidative decomposition of the phenothiazine group through the opening of the ring structure. After 45 min of photocatalytic degradation, the absorbance of the solution was close to zero and it was completely colorless, thus, indicating total MB degradation.

In addition to photocatalysis, photolysis was also evaluated to verify the effect of light on the degradation of MB separately, hence, providing further insights into the influence of the catalyst on the degradation. Moreover, catalysis and photocatalysis experiments were performed using the PR catalyst and the results were compared to those of the PR-Fc, as shown in Fig. 4.

The decay of the absorption of light by MB as a function of time is shown in Fig. 4(B) for each system studied. All evaluated processes were able to discolor the dye, except for the one performed with PR, which did not promote MB discoloration. A significant improvement in the degradation of MB was observed for the PR-Fc catalyst when compared to PR, both in the absence and incidence of light. Degradation is faster and more efficient by combining the PR-Fc catalyst and UV–vis light. MB degradation can be modeled as a pseudo first-order reaction. Degradation kinetics calculated for the initial 30 min of reaction are expressed by the equation: $-\ln(A / A_0) = kt$, where A_0 is the initial absorbance, A is the absorbance at each reaction time, t (min), and k is the reaction rate constant. First order kinetics was the most appropriate model to show the MB degradation kinetics with the different catalysts. The rate constants shown in Fig. 4(C) were obtained from linear extrapolations. The rate constants for photolysis, PR catalysis and PR-UV–vis photocatalysis were 3.66×10^{-2} min^{-1}, 0.04×10^{-2} min^{-1} and 5.97 10^{-2} min^{-1}, respectively, while those for PR catalysis and PR-Fc photocatalysis were 1.74×10^{-2} min^{-1} and 7.58×10^{-2} min^{-1}, respectively.

To investigate whether MB degradation was only a result of chromophoric breakage, leading to a simple discoloration process, or of dye mineralization, TOC measurements were performed after the

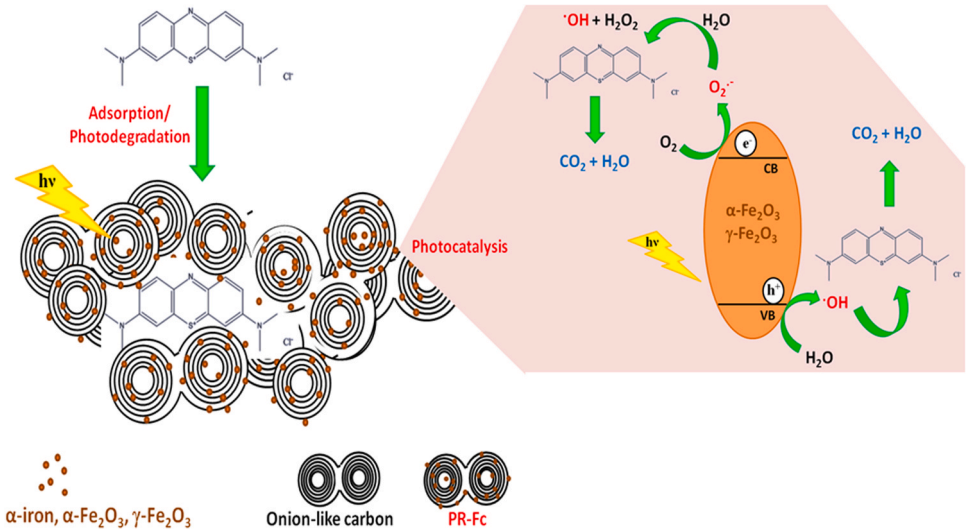

Fig. 5. Schematic illustration of proposed mechanisms for MB degradation through the PR-Fc catalyst.

degradation experiments.

Fig. 4(D) shows the results of MB removal percentage after 60 min of degradation through photolysis, catalysis and photocatalysis.

Light irradiation alone was not able to remove the organic load from the solution. Moreover, MB removal was not observed in PR catalysis. In the photocatalysis experiments, the PR catalyst removed 55% of MB, which shows that the incidence of light upon the carbonaceous material might have promoted an increase in dye adsorption onto the surface of the material and, as a result, the total organic carbon decayed in the solution. On the other hand, the PR-Fc catalyst alone removed 75% of MB. The onion-like activated carbon structures of the PR-Fc catalyst can promote MB adsorption, removing it from the solution, which explains a high removal rate in the absence of light. Furthermore, this material has a high surface area compared to PR, which can improve the adsorption process. However, MB degradation is not only associated with the adsorption process, as the PR-Fc structure contains iron oxides in different phases and of distinct photoactive characteristics [60]. In photocatalysis, the combination of the PR-Fc catalyst and light achieved 97% of dye removal from the solution in just 60 min.

The high MB removal rate using the PR-Fc catalyst can be explained by two factors. First, the developed catalyst has a high surface area and various adsorption sites, hence, it can adsorb dye molecules through the iron oxides present in its structure. MB adsorption can occur via p - p orbital conjugation between the MB molecules and the aromatic regions of the carbonaceous catalyst [7]. Dye photodegradation and direct charge transfer from PR-Fc to the MB adsorbed on the active catalyst surface was achieved through the incidence of light. Second, under illumination, the Fe_2O_3 valence band (VB) electrons present in the catalyst are excited to the conduction band (CB) and the electron-hole pair is formed as a result. As the carbon surface is highly conductive, it can accept electrons photogenerated by the iron oxides and promote both a rapid movement of charges and their separation [9]. The increased charge transport induces the formation of more photo-induced carriers for photocatalytic reactions, thus, enhancing the photocatalytic activity of the material. The photogenerated electrons of Fe_2O_3 can still react with oxygen dissolved in the solution and generate superoxide radical ($O_2^{\bullet-}$) anions, moreover, the holes lead to the formation of hydroxyl radicals ($^{\bullet}OH$) that assist in the oxidation of organic compounds [13]. Thus, MB degradation can occur via the adsorption of the dye and photodegradation on the catalyst surface, hence, oxidation is promoted by charge carriers photogenerated by the iron oxides. The proposed mechanism of MB degradation for the PR-Fc catalyst under light

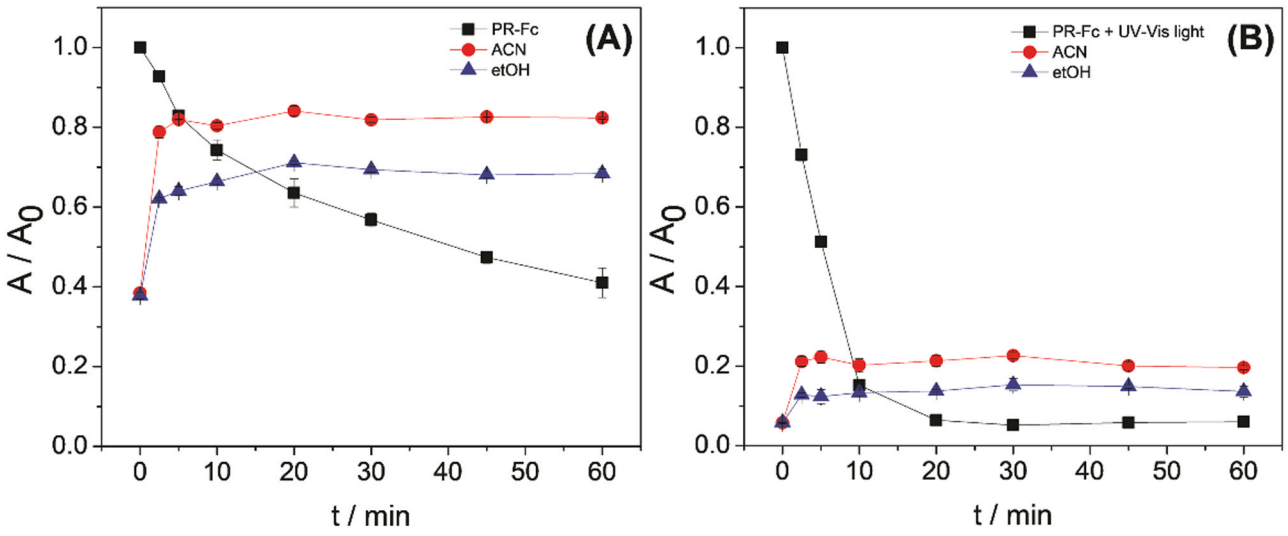

Fig. 6. Adsorption study for MB interacting with the PR-Fc catalyst in the absence (A) and presence of light (B); desorption experiments using acetonitrile (ACN) and ethanol (etOH). The error bars correspond to two repetitions.

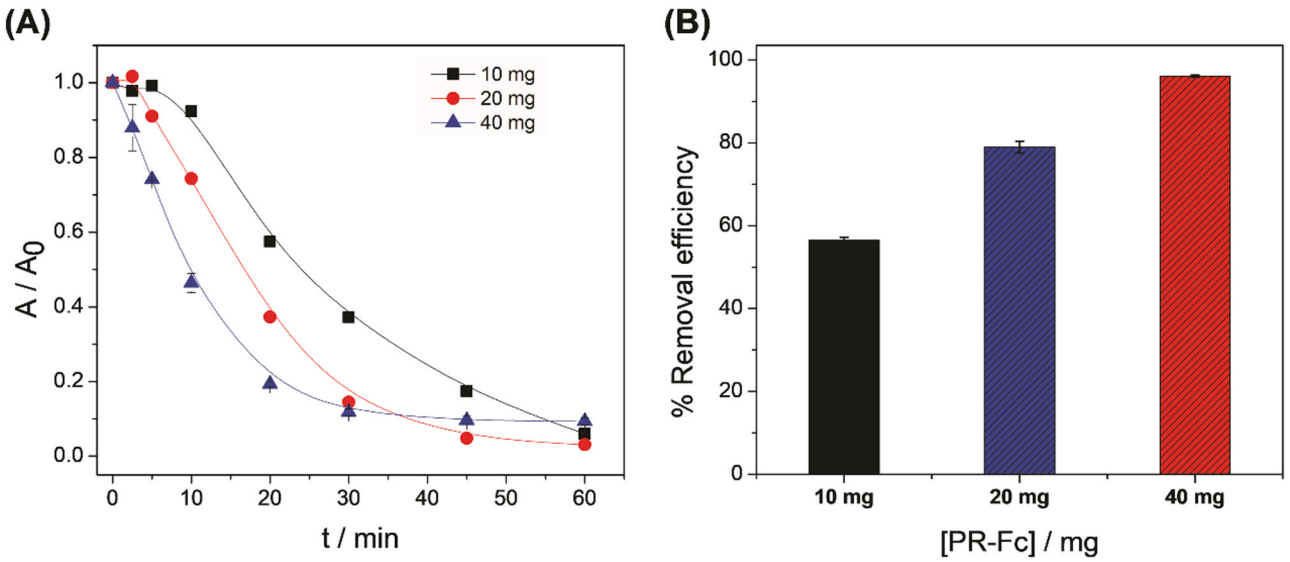

Fig. 7. (A) Photodegradation of MB and (B) corresponding TOC removal (%) using different masses of the PR-Fc catalyst (10, 20 and 40 mg) during 60 min. The error bars correspond to two repetitions.

irradiation is presented in Fig. 5.

The adsorption capacity of the PR-Fc catalyst was studied during MB degradation experiments both in the absence and presence of light. These experiments were performed in order to verify if the catalyst simply adsorbs MB, removing it from the solution, or if there is photoactivation of iron species in its structure, which assists in the photocatalysis, as proposed above. Fig. 6 shows the results of adsorption obtained in the absence (Fig. 6(A)) and in the presence of light (Fig. 6 (B)), as well as desorption experiments performed using acetonitrile (ACN) and ethanol (etOH). As it can be seen, the absorbance decay of MB is about 70% after 60 min in the absence of light, which was associated with the material adsorption process, since desorption of part of the MB contained on the catalyst surface was verified when acetonitrile and ethanol reagents were added into the solution. The best reagent to desorb MB from PR-Fc was acetonitrile when compared to ethanol, desorbing 72% and 48%, respectively, after 60 min of analysis. However, there was a synergistic effect related to the light and the catalyst on the MB removal with the incidence of light. The absorbance decay was almost 100%, moreover, 97% of the total organic load was removed from the solution, as observed in TOC tests.

After the desorption tests, only 14% of the MB was desorbed in acetonitrile after photocatalysis, indicating a significant increase in the degradation of the dye through photoactivation of the catalyst. From the quotient between the percentages of MB desorbed from PR-Fc using acetonitrile in the presence and absence of light, the contribution of photocatalysis during the degradations was estimated. The coefficient of synergistic effect for PR-Fc was about 5.14 (explicitly, 5.14 = 72%/14%) in the presence of light, i.e. the degradation of the compound was about 5 times greater in the presence of light compared to catalysis in the dark. This indicates that MB degradation is a process of adsorption and photocatalysis with activation of the iron catalyst species through the incidence of light, as mentioned above.

3.3. Effect of PR-Fc mass

The effect of the PR-Fc catalyst mass on the photocatalysis process was evaluated; the assays were performed using a 25 mg L^{-1} MB solution for 60 min of reaction time evaluating the performance of 10, 20 and 40 mg of PR-Fc. The quantity of catalyst studied was chosen based on the catalyst materials containing iron and carbon oxides reported in the literature [10,13,61]. Fig. 7(A) shows the A/A_0 versus time for each catalyst mass. It can be observed that all studied catalyst masses promoted MB degradation. However, the slowest reaction rate was achieved when photocatalysis was performed with 10 mg PR-Fc, as a complete dye discoloration was only achieved after 60 min. Increasing the mass to 20 mg, a complete dye discoloration was achieved after 45 min. The fastest MB degradation rate was obtained for photocatalysis experiments using 40 mg PR-Fc. Generally, an increase in catalyst mass increases the solution turbidity and may decrease the degradation of compounds, since the penetration of light can decrease due to the amount of suspended particles [62]. However, for the tested masses up to 40 mg of PR-Fc, the synergistic effect between catalyst and light can be observed in photocatalysis without significant interference from the turbidity of the solution.

The MB removal efficiency was assessed by TOC measurements and the results are shown in Fig. 7(B). 57% of dye removal was achieved using 10 mg of PR-Fc, 80% using 20 mg and 97% using 40 mg of PR-Fc. This shows that it is possible to remove more than half of the MB in just

Table 1
Advanced Oxidation Processes to remove dyes from wastewater.

(Catalyst/ Oxidants)	[Dye] (mg L^{-1})	[Catalyst] (g L^{-1})	Color removal (%)	Time (min)	Ref
oxide-supported metal activated carbon	100	0.20	100[a]	75	[7]
CNT/TiO_2/ AgNPs/ Surfactant	20.0	0.50	100%[a]	180	[16]
Carbon xerogel/ CNT-Ti	10.0	0.02	90–99%[a]	60	[17]
Ag@ AgBr (20% wt)/ Bi_2WO_6	10.0	1.00	99[a]	60	[26]
ZnO/UV	50.0	6.00	76[a]	120	[27]
α-Fe_2O_3	10.0	1.00	89[a]	140	[28]
SiO_2@α-Fe_2O_3 on SnS_2 flowers	5.00	0.40	96[a]	100	[13]
Fe+H_3BO_3/ α-Fe_2O_3	10.0	0.07	96[a]	120	[29]
Fe_2O_3/AC/ polyester fibers	0.6–16	0.10	96–98%[a]	60	[30]
ZnO/SnO_2	10.0	0.50	96[a]	60	[31]
SnO_2/α-Fe_2O_3	5.00	0.40	98[a]	240	[32]
This work	25.0	0.40	100 ± 0.01[b]	60	–

[a] references do not mention standard deviations.
[b] 97% organic load removal (60 min); ± 0.01(standard deviation).

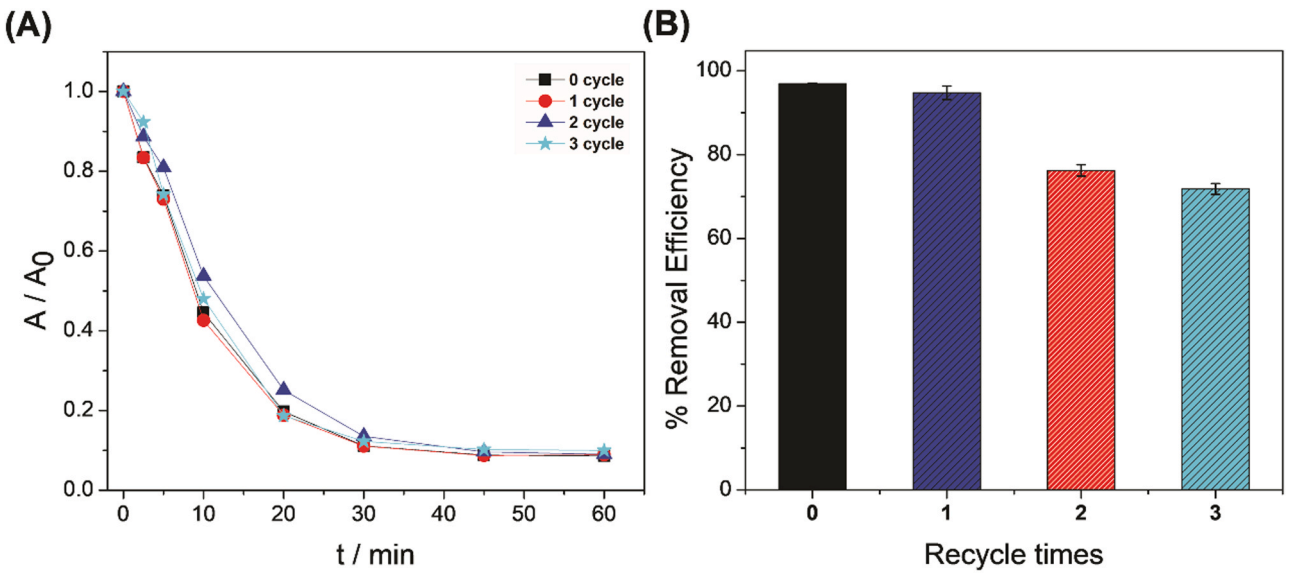

Fig. 8. (A) Photodegradation of MB using PR-Fc and (B) corresponding TOC removal (%) demonstrating catalyst reusability. The error bars correspond to two repetitions.

60 min, even at low catalyst concentrations. Experiments involving greater catalyst masses were not performed, since 97% of the dye was completely removed using 40 mg of PR-Fc. Thus, 40 mg of PR-Fc was selected for further experiments.

The results discussed herein indicate that the developed catalyst presents a high catalytic capacity compared to other carbon and oxide materials, as shown in the Table 1.

3.4. Reusability test

The stability and durability of the PR-Fc were evaluated through recycling experiments, shown in Fig. 8. In all experiments, there was complete dye discoloration upon reutilization of the catalyst, as can be seen in Fig. 8(A). It was observed that the first catalyst reuse is as efficient as the initial catalyst, since the MB removal rate was the same as in photocatalysis measurements after 60 min. From the second cycle, there is a 23% decrease of the catalytic efficiency and a stabilization of the catalytic efficiency occurs in the third reuse cycle. These results prove the efficiency of the catalyst in the degradation of MB and its possible reuse with 100% efficiency in the first cycle. Although the efficiency of MB removal decreases to around 80% after the second cycle, PR-Fc has the advantage of being a low-cost and easily synthesized catalyst. Thus, the reuse of this catalyst for several cycles or the use of the catalyst only once would not have a major economic impact when compared to other materials proposed in the literature that have longer and more expensive syntheses [13,63,64].

Hematite (α-Fe_2O_3) has a rhombohedral structure and weak ferromagnetic and antiferromagnetic properties. Maghemite (γ-Fe_2O_3) has an inverse spinel structure and ferrimagnetic properties [65]. Furthermore, these magnetic materials can contribute to both adsorption efficiency and photodegradation with high stability and great capacity for reuse, in addition to the ease of removal from the solution by magnetic systems after the experiments. A similar material produced in a previous study [37] was tested to remove atrazine from wastewater and the photocatalyst showed great efficiency.

4. Conclusions

Onion-like carbon structures have been successfully designed and modified using heat-treated iron oxides. The PR-Fc material showed high photocatalytic activity while degrading MB dye if compared to results of PR and those of similar studies. In PR-Fc photocatalysis, 97% of the organic load was removed from the solution in just 60 min. According to adsorption and desorption measurements using acetonitrile and ethanol as solvents, it is suggested that the removal of MB through the PR-Fc catalyst is a process of coupled adsorption and photocatalysis, then, a degradation mechanism is proposed. In addition to high efficiency in MB photocatalysis, the PR-Fc catalyst showed high stability and great capacity for reuse, in addition to the great advantage of being a magnetic material, which facilitates its removal from the solution by magnetic systems after experiments. Due to its low cost, easy synthesis, photoactive characteristics and reuse capabilities, the PR-Fc catalyst can potentially be employed as a photoactive catalyst in emerging pollutant treatments.

CRediT authorship contribution statement

Roberto Bertholdo: Conceptualization and methodology, BET analysis. **Lucia Helena Mascaro Sales:** Conceptualization and methodology, BET analysis. **Carmen Greice Renda:** Phenolic resin and onion-like carbon synthesis and characterization of catalysts. **Lorena Athie Goulart:** Photocatalytic activity test and discussion about mechanism. **Jose Mario de Aquino:** Reusability test. **Carlos Henrique Magalhaes Fernandes:** Reusability test.

All authors: discussions and conclusions.

Declaration of Competing Interest

The authors declare that they have no known competing financial interests or personal relationships that could have appeared to influence the work reported in this paper.

Acknowledgments

Authors acknowledge the São Paulo Research Foundation (FAPESP) for financial support to the project and for the fellowships granted (grants number #2018/16401-8, #2017/11986-5, #2014/50249-8, #2013/07296-2). The authors also thank the Coordenação de Aperfeiçoamento de Pessoal de Nível Superior (CAPES) - Finance Code 001, the Conselho Nacional de Pesquisa e Desenvolvimento (CNPq).

References

[1] J. Wang, S. Wang, Activation of persulfate (PS) and peroxymonosulfate (PMS) and application for the degradation of emerging contaminants, Chem. Eng. J. 334 (2018) 1502–1517, https://doi.org/10.1016/j.cej.2017.11.059.

[2] T. Rasheed, M. Bilal, F. Nabeel, M. Adeel, H.M.N. Iqbal, Environmentally-related contaminants of high concern: Potential sources and analytical modalities for detection, quantification, and treatment, Environ. Int. 122 (2019) 52–66, https://doi.org/10.1016/j.envint.2018.11.038.

[3] K. Sharma, R.K. Vyas, A.K. Dalai, Thermodynamic and kinetic studies of methylene blue degradation using reactive adsorption and its comparison with adsorption, J. Chem. Eng. Data 62 (2017) 3651–3662, https://doi.org/10.1021/acs.jced.7b00379.

[4] X. Wu, P. Xiao, S. Zhong, K. Fang, H. Lin, J. Chen, Magnetic $ZnFe_2O_4$@chitosan encapsulated in graphene oxide for adsorptive removal of organic dye, RSC Adv. 7 (2017) 28145–28151, https://doi.org/10.1039/c7ra04100d.

[5] K. Chen, J. Wu, C. Huang, Y. Liang, S.J. Hwang, Decolorization of azo dye using PVA-immobilized microorganisms, J. Biotechnol. 101 (2003) 241–252, https://doi.org/10.1016/S0168-1656(02)00362-0.

[6] R. Gong, Y. Ding, M. Li, C. Yang, H. Liu, Y. Sun, Utilization of powdered peanut hull as biosorbent for removal of anionic dyes from aqueous solution, Dyes Pigment. 64 (2005) 187–192, https://doi.org/10.1016/j.dyepig.2004.05.005.

[7] A. Nasrollahpour, S.E. Moradi, Photochemical degradation of methylene blue by metal oxide-supported activated carbon photocatalyst, Desalination Water Treat. 57 (2016) 8854–8862, https://doi.org/10.1080/19443994.2015.1035675.

[8] Ö. Gökkuş, Oxidative degradation of Basic Black 3 by electro-generated Fenton's reagent using carbon fiber cathode, Clean Technol. Environ. Policy 18 (2016) 1525–1534, https://doi.org/10.1007/s10098–016-1134-y.

[9] T.A. Saleh, V.K. Gupta, Photo-catalyzed degradation of hazardous dye methyl orange by use of a composite catalyst consisting of multi-walled carbon nanotubes and titanium dioxide, J. Colloid Interface Sci. 371 (2012) 101–106, https://doi.org/10.1016/j.jcis.2011.12.038.

[10] A.N. Soon, B.H. Hameed, Heterogeneous catalytic treatment of synthetic dyes in aqueous media using Fenton and photo-assisted Fenton process, Desalination 269 (2011) 1–16, https://doi.org/10.1016/j.desal.2010.11.002.

[11] H. Kusic, N. Koprivanac, L. Srsan, Azo dye degradation using Fenton type processes assisted by UV irradiation: a kinetic study, J. Photochem. Photobiol. A Chem. 181 (2006) 195–202, https://doi.org/10.1016/j.jphotochem.2005.11.024.

[12] A.G. Gutierrez-Mata, S. Velazquez-Martínez, A. Álvarez-Gallegos, M. Ahmadi, J. A. Hernández-Pérez, F. Ghanbari, S. Silva-Martínez, Recent overview of solar photocatalysis and solar photo-fenton processes for wastewater treatment, Int. J. Photoenergy (2017), 8528063, https://doi.org/10.1155/2017/8528063.

[13] S. Balu, K. Uma, G. Pan, T.C.-K. Yang, S.K. Ramaraj, Degradation of methylene blue dye in the presence of visible light using SiO2@alfa-Fe2O3 nanocomposites deposited on SnS2 flowers, Materials (2018), 1030, https://doi.org/10.3390/ma11061030.

[14] A.O. Ibhadon, P. Fitzpatrick, Heterogeneous photocatalysis: recent advances and applications, Catalysis 3 (2013) 189–218, https://doi.org/10.3390/catal3010189.

[15] M.A. Abid, D.A. Kadhim, Novel comparison of iron oxide nanoparticle preparation by mixing iron chloride with henna leaf extract with and without applied pulsed laser ablation for methylene blue degradation, J. Environ. Chem. Eng. 8 (2020), 104138, https://doi.org/10.1016/j.jece.2020.204138.

[16] E.M.S. Azzam, N.A. Fathy, S.M. El-Khouly, R.M. Sami, Enhancement the photocatalytic degradation of methylene blue dye using fabricated CNTs/TiO_2/AgNPs/Surfactant nanocomposites, J. Water Process Eng. 28 (2019) 311–321, https://doi.org/10.1016/j.jwpe.2019.02.016.

[17] N.A. Fathy, S.M. El-Khouly, R.M.M. Aboelenin, Carbon xerogel/carbon nanotubes nanohybrid doped with Ti for removal of methylene blue dye, Egypt. J. Chem. 62 (2019) 2277–2288, https://doi.org/10.21608/ejchem.2019.12870.1803.

[18] F. Chen, X. Wu, L. Yang, C. Chen, H. Lin, J. Chen, Efficient degradation and mineralization of antibiotics via heterogeneous activation of peroxymonosulfate by using graphene supported single-atom Cu catalyst, Chem. Eng. J. 394 (2020), 124904, https://doi.org/10.1016/j.cej.2020.124904.

[19] D. Zhao, G. Sheng, C. Chen, X. Wang, Enhanced photocatalytic degradation of methylene blue under visible irradiation on graphene@TiO_2 dyade structure, Appl. Catal. B Environ. 111–112 (2012) 303–308, https://doi.org/10.1016/j.apcatb.2011.10.012.

[20] A.G.B. Pereira, F.H.A. Rodrigues, A.T. Paulino, A.F. Martins, A.R. Fajardo, Recent advances on composite hydrogels designed for the remediation of dye-contaminated water and wastewater: a review, J. Clean. Prod. (2020), 124703, https://doi.org/10.1016/j.jclepro.2020.124703.

[21] M. Zhou, Q. Li, S. Zhong, J. Chen, H. Lin, X. Wu, Facile large scale fabrication of magnetic carbon nano-onions for efficient removal of bisphenol A, Mater. Chem. Phys. 198 (2017) 186–192, https://doi.org/10.1016/j.matchemphys.2017.05.020.

[22] A. Garmroudi, M. Kheirollahi, S.A. Mousavi, M. Fattahi, E.H. Mahvelati, Effects of graphene oxide/TiO_2 nanocomposite, graphene oxide nanosheets and Cedr extraction solution on IFT reduction and ultimate oil recovery from a carbonated rock, Colloids Surf. A Physicochem. Eng. Asp. (2020), https://doi.org/10.1016/j.petlm.2020.10.002. PII: S2405-6561(20)30099-7.

[23] S. Naeem, V. Baheti, J. Militky, J. Wiener, P. Behera, A. Ashraf, Sorption properties of iron impregnated activated carbon web for removal of methylene blue from aqueous media, Fibers Polym. 17 (2016) 1245–1255, https://doi.org/10.1007/s12221-016-6423-x.

[24] T.E. Rufford, D. Hulicova-Jurcakova, Z. Zhu, G.Q. Lu, A comparative study of chemical treatment by $FeCl_3$, $MgCl_2$, and $ZnCl_2$ on microstructure, surface chemistry, and double-layer capacitance of carbons from waste biomass, Mater. Res. Soc. 25 (2010) 1451–1459, https://doi.org/10.1557/JMR.2010.0186.

[25] S.K. Theydan, M.J. Ahmed, Adsorption of methylene blue onto biomass-based activated carbon by $FeCl_3$ activation: equilibrium, kinetics, and thermodynamic studies, J. Anal. Appl. Pyrolysis 97 (2012) 116–122, https://doi.org/10.1016/j.jaap.2012.05.008.

[26] S. Lin, L. Liu, J. Hu, Y. Liang, W. Cui, Nano Ag@AgBr surface-sensitized Bi_2WO_6 photocatalyst: oil-in-water synthesis and enhanced photocatalytic degradation, Appl. Surf. Sci. 324 (2015) 20–29, https://doi.org/10.1016/j.apsusc.2014.10.101.

[27] S. Chakrabarti, B.K. Dutta, Photocatalytic degradation of model textile dyes in wastewater using ZnO as semiconductor catalyst, J. Hazard. Mater. B112 (2004) 269–278, https://doi.org/10.1016/j.jhazmat.2004.05.013.

[28] A. Lassoued, M.S. Lassoued, B. Dkhil, S. Ammar, A. Gadri, Photocatalytic degradation of methylene blue dye by iron oxide (α-Fe_2O_3) nanoparticles under visible irradiation, J. Mater. Sci. Mater. Electron. 29 (2018) 8142–8152, https://doi.org/10.1007/s10854-018-8819-4.

[29] R. Edla, A. Tonezzer, M. Orlandi, N. Patel, R. Fernandes, N. Bazzanella, K. Date, D. C. Kothari, A. Miotello, 3D hierarchical nanostructures of iron oxides coatings prepared by pulsed laser deposition for photocatalytic water purification, Appl. Catal. B Environ. 219 (2017) 401–411, https://doi.org/10.1016/j.apcatb.2017.07.063.

[30] Z.C. Kadirova, M. Hojamberdiev, K.- Katsumata, T. Isobe, N. Matsushita, A. Nakajima, K. Okada, Fe_2O_3-loaded activated carbon fiber/polymer materials and their photocatalytic activity for methylene blue mineralization by combined heterogeneous-homogeneous photocatalytic processes, Appl. Surf. Sci. 402 (2017) 444–455, https://doi.org/10.1016/j.apsusc.2017.01.131.

[31] Y. Chiang, C. Lin, Photocatalytic decolorization of methylene blue in aqueous solutions using coupled ZnO/SnO_2 photocatalysts, Powder Technol. 246 (2013) 137–143, https://doi.org/10.1016/j.powtec.2013.04.033.

[32] S. Zhang, J. Li, H. Niu, W. Xu, J. Xu, W. Hu, X. Wang, Visible-light photocatalytic degradation of methylene blue using SnO_2/α-Fe_2O_3 hierarchical nanoheterostructures, Chempluschem 78 (2013) 192–199, https://doi.org/10.1002/cplu.201200272.

[33] Q. Lin, Z. Feng, Z. Liu, Q. Guo, Z. Hu, L. He, H. Ye, Atomic scale investigations of catalyst and catalytic graphitization in a silicon and titanium doped graphite, Carbon 88 (2015) 252–261, https://doi.org/10.1016/j.carbon.2015.03.001.

[34] S. Wang, L. Qiao, C. Zhao, X. Zhang, J. Chen, H. Tian, W. Zheng, Z. Han, A growth mechanism for graphene deposited on polycrystalline Co film by plasma enhanced chemical vapor deposition, R. Soc. Chem. 37 (2013) 1616–1622, https://doi.org/10.1039/C3NJ41136B.

[35] M. Rezaee, M. Kazemeini, M. Fattahi, A.M. Rashidi, L. Vafajoo, Oxidation of H_2S to elemental sulfur over alumina-based nanocatalysts: synthesis and physiochemical evaluations, Sci. Iran. 23 (2016) 1160–1174, https://doi.org/10.24200/sci.2016.3886.

[36] M. Kazemeini, M. Nikkhah, M. Fattahi, L. Vafajoo, Physicochemical properties and catalytic performances of nanostructured V_2O_5 over TiO_2 and γ-Al_2O_3 for oxidative dehydrogenation of propane, Chem. Biochem. Eng. Q. 30 (2016) 9–18, https://doi.org/10.15255/CABEQ.2014.2049.

[37] C.G. Renda, C.P. Contreras Medrano, L.J.D. Costa, F.J. Litterst, E.M.B. Saitovitch, C.J. Magon, A.J. Gualdi, T. Venâncio, R. Bertholdo, A.J. Moreira, G.P.G. Freschi, A. A. Lucas, Role of ferrocene-derived iron species in the catalytic graphitization of novolak resins, J. Mater. Sci. 05312 (2020) 1–14, https://doi.org/10.1007/s10853-020-05312-z.

[38] K.M. Reza, A.S.W. Kurny, F. Gulshan, Parameters affecting the photocatalytic degradation of dyes using TiO_2: a review, Appl. Water Sci. 7 (2017) 1569–1578, https://doi.org/10.1007/s13201-015-0367-y.

[39] C.G. Renda, R. Bertholdo, Study of phenolic resin and their tendency for carbon graphitization, J. Polym. Res. 25 (2018), 241, https://doi.org/10.1007/s10965-018-1635-y.

[40] A.P. Luz, C.G. Renda, A.A. Lucas, R. Bertholdo, C.G. Aneziris, V.C. Pandolfelli, Graphitization of phenolic resins for carbon-based refractories, Ceram. Int. 43 (2017) 8171–8182, https://doi.org/10.1016/j.ceramint.2017.03.143.

[41] C.G. Renda, R. Bertholdo, T. Venâncio, A.P. Luz, V.C. Pandolfelli, A.A. Lucas, Influence of the mixing process on the graphitization of phenolic resins, Ceram. Int. 45 (2019) 12196–12204, https://doi.org/10.1016/j.ceramint.2019.03.124.

[42] J. Tauc, R. Grigorovici, A. Vancu, Optical properties and electronic structure of amorphous Ge, Phys. Status Solid 15 (1966) 627–637, https://doi.org/10.1002/pssb.19660150224.

[43] M. Zhao, H. Song, Catalytic graphitization of phenolic resin, J. Mater. Sci. Technol. 27 (2011) 266–270, https://doi.org/10.1016/S1005-0302(11)60060-1.

[44] A. Oya, H. Marsh, Phenomena of catalytic graphitization, J. Mater. Sci. 17 (1982) 309–322, https://doi.org/10.1007/BF00591464.

[45] M.I. Dar, S.A. Shivashankar, Single crystalline magnetite, maghemite, and hematite nanoparticles with rich coercivity, R. Soc. Chem. 4 (2014) 4105–4113, https://doi.org/10.1039/c3ra45457f.

[46] I. Stamatin, A. Morozan, A. Dumitru, V. Ciupina, G. Prodan, J. Niewolski, H. Figiel, The synthesis of multi-walled carbon nanotubes (MWNTs) by catalytic pyrolysis of the phenol-formaldehyde resins, Physica E 37 (2007) 44–48, https://doi.org/10.1016/j.physe.2006.10.013.

[47] D.C. Silva, L.R.P. Kassab, J.R. Martinelli, A.D. Santos, S.J.L. Ribeiro, M.V. Santos, Characterization of thin carbon films produced by the magnetron sputtering technique, Mater. Res. 19 (2016) 669–672, https://doi.org/10.1590/1980-5373-MR-2015-0058.

[48] Z. Gong, C. Bai, L. Qiang, K. Gao, J. Zhang, B. Zhang, Onion-like carbon films endow macro-scale superlubricity, Diam. Relat. Mater. 87 (2018) 172–176, https://doi.org/10.1016/j.diamond.2018.06.004.

[49] M. Thommes, K. Kaneko, A.V. Neimark, J.P. Olivier, F. Rodriguez-Reinoso, J. Rouquerol, K.S.W. Sing, Physisorption of gases, with special reference to the evaluation of surface area and pore size distribution (IUPAC Technical Report), Pure Appl. Chem. 87 (2015) 1051–1069, https://doi.org/10.1515/pac-2014-1117.
[50] S. Cheng, L. Zhang, A. Ma, H. Xia, J. Peng, C. Li, J. Shu, Comparison of activated carbon and iron/cerium modified activated carbon to remove methylene blue from wastewater, J. Environ. Sci. 65 (2018) 92–102, https://doi.org/10.1016/j.jes.2016.12.027.
[51] N.A.M. Barakat, Synthesis and characterization of maghemite iron oxide (γ-Fe_2O_3) nanofibers: novel semiconductor with magnetic feature, J. Mater. Sci. 47 (2012) 6237–6245, https://doi.org/10.1007/s10853-012-6543-7.
[52] C. Hao, F. Feng, X. Wang, M. Zhou, Y. Zhao, C. Ge, K. Wang, The preparation of Fe_2O_3 nanoparticles by liquid phase-based ultrasonic-assisted method and its application as enzyme-free sensor for the detection of H_2O_2, RSC Adv. 5 (2015) 21161–21169, https://doi.org/10.1039/c4ra17226d.
[53] R.A. Bepari, P. Bharali, B.K. Das, Controlled synthesis of alpha- and γ-Fe_2O_3 nanoparticles via thermolysis of PVA gels and studies on α-Fe_2O_3 catalyzed styrene epoxidation, J. Saudi Chem. Soc. 21 (2014) S170–S178, https://doi.org/10.1016/j.jscs.2013.12.010.
[54] R.S. Jack, G.A. Ayoko, M.O. Adebajo, R.L. Frost, A review of iron species for visible-light photocatalyst water purification, Environ. Sci. Pollut. Res. 22 (2015) 7439–7449, https://doi.org/10.1007/s11356-015-4346-5.
[55] S. Chen, G. Yang, C. Wang, S. Yang, D. Chen, X. Cai, Y. Li, F. Pen, Y. Fang, S. Zhang, Magnetic Fe_3C@C nanoparticles as a novel cocatalyst for boosting visible-light-driven photocatalytic performance of g-C_3N_4, Int. J. Hydrog. Energy 44 (2019) 26970–26981, https://doi.org/10.1016/j.ijhydene.2019.08.150.
[56] V.A.R. Villegas, J.I.L. Ramirez, E.H. Guevara, S.P. Sicairos, L.A.H. Ayala, B. L. Sanchez, Synthesis and characterization of magnetite nanoparticles for photocatalysis of nitrobenzene, J. Saudi Chem. Soc. 24 (2019) 223–235, https://doi.org/10.1016/j.jscs.2019.12.004.
[57] Z. Yang, C. Zhang, G. Zeng, X. Tan, H. Wang, D. Huang, K. Yang, J. Wei, C. Ma, K. Nie, Design and engineering of layered double hydroxide based catalysts for water depollution by advanced oxidation processes: a review, J. Mater. Chem. A 8 (2020) 4141–4173, https://doi.org/10.1039/C9TA13522G.
[58] R.S. Dariani, A. Esmaeili, A. Mortezaali, S. Dehghanpour, Photocatalytic reaction and degradation of methylene blue on TiO_2 nano-sized particles, Optik 127 (2016) 7143–7154, https://doi.org/10.1016/j.ijleo.2016.04.026.
[59] J. Lin, Z. Luo, J. Liu, P. Li, Photocatalytic degradation of methylene blue in aqueous solution by using ZnO-SnO_2 nanocomposites, Mater. Sci. Semicond. Process. 87 (2018) 24–31, https://doi.org/10.1016/j.mssp.2018.07.003.
[60] M. Barroso, A.J. Cowan, S.R. Pendlebury, M. Grätzel, D.R. Klug, J.R. Durrant, The role of cobalt phosphate in enhancing the photocatalytic activity of alfa-Fe_2O_3 toward water oxidation, J. Am. Chem. Soc. 133 (2011) 14868–14871, https://doi.org/10.1021/ja205325v.
[61] O. Turgay, G. Ersoz, S. Atalay, J. Forss, U. Welander, The treatment of azo dyes found in textile industry wastewater by anaerobic biological method and chemical oxidation, Sep. Purif. Technol. 79 (2011) 26–33, https://doi.org/10.1016/j.seppur.2011.03.007.
[62] R. Wu, C. Chen, M. Chen, C. Lu, Titanium dioxide-mediated heterogeneous photocatalytic degradation of terbufos: parameter study and reaction pathways, J. Hazard. Mater. 162 (2009) 945–953, https://doi.org/10.1016/j.jhazmat.2008.05.121.
[63] P. Saikia, A.T. Miah, P.P. Das, Highly efficient catalytic reductive degradation of various organic dyes by Au/CeO2-TiO2 nano-hybrid, J. Chem. Sci. 129 (2017) 81–93, https://doi.org/10.1007/s12039-016-1203-0.
[64] A.M. Atta, Y.M. Moustafa, H.A. Al-Lohedan, A.O. Ezzat, A.I. Hashem, Methylene blue catalytic degradation using silver and magnetite nanoparticles functionalized with a poly(ionic liquid) based on quaternized dialkylethanolamine with 2-acrylamido-2-methylpropane sulfonate- co-vinylpyrrolidone, ACS Omega 5 (6) (2020) 2829–2842, https://doi.org/10.1021/acsomega.9b03610.
[65] R.M. Cornell, U. Schwertmann, The Iron Oxides: Structure, Properties, Reactions, Occurrences and Uses, Secon, Com, Willey VCH Verlag GmbH & Co, Weinheim, 2003.